THE JOURNAL OF PHYSICAL CHEMISTRY C
A JOURNAL OF THE AMERICAN CHEMICAL SOCIETY

pubs.acs.org/JPCC

Article

Unraveling the Hydroxide Ion Transportation Mechanism along the Surface of Two-Dimensional Layered Double Hydroxide Nanosheets

Le Shi,* Zhixuan Ying, Ao Xu, and Yonghong Cheng

Cite This: *J. Phys. Chem. C* 2021, 125, 1240–1248

Read Online

ACCESS | Metrics & More | Article Recommendations | Supporting Information

ABSTRACT: Traditional polymeric anion exchange membranes (AEMs) suffer from longstanding issues such as low ionic conductivities, poor stability, and high toxic preparation procedures. Recent experiments demonstrated that exfoliated two-dimensional layered double hydroxide (2D-LDH) could provide a super high hydroxide ion conductivity of about 0.1 S/cm, which is 1 to 2 orders of magnitude higher than that of commercial AEMs. However, the hydroxide ion conduction mechanism of this material is still unclear. Our ab initio molecular dynamics (AIMD) simulation results reveal that the positively charged 2D-LDH slab ($Mg_2Al(OH)_6^+$) can induce a quasi-two-dimensional hydroxide ion transportation behavior along the surface of 2D-LDH with a diffusivity comparable with that in the bulk water environment. When restacking 2D-LDH nanosheets, the spatial confinement will destroy the connectivity of the hydrogen bonding network and hamper the hydroxide ion conduction capability. The hydroxyl functional groups on 2D-LDH can mediate the hydroxide ion transportation process between non-adjacent water molecules with a relatively high energy barrier, which can only be activated in low humidity conditions. Our results shed light on future designs of stable anion exchange membranes based on inorganic 2D materials.

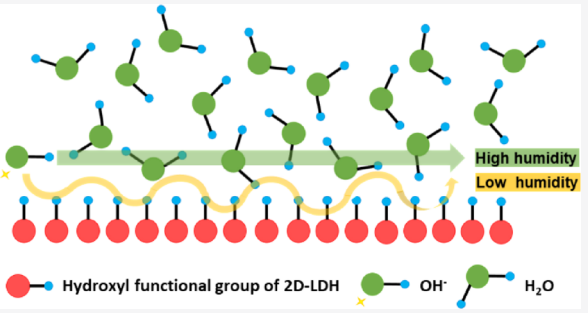

1. INTRODUCTION

Anion exchange membranes (AEMs) play a vital role in many renewable energy and bioelectronic devices, such as fuel cells, water electrolysers, and sensors.[1−3] For example, most current fuel cell technologies operate in an acidic environment and require the usage of a noble metal catalyst. With satisfying-performed AEMs, the operation conditions of fuel cells can shift to an alkaline environment, where much cheaper and abundant non-precious metal catalysts can be employed.[4,5] Most of the commercial AEMs consist of hydrocarbon mainchains connecting quaternary ammonium functional groups that can conduct hydroxide anions. The preparation of polymeric AEMs involves highly toxic procedures, and the quaternary ammonium functional groups suffer from poor thermal and chemical stability.[6] On the other hand, the typical ionic conductivity of commercial AEMs is only about 10^{-3} to 10^{-2} S/cm[7], which is one or two magnitudes lower than that of commercial proton exchange membranes. Therefore, the development of next-generation environmental-friendly AEMs that can provide high ionic conductivity as well as good thermal and chemical stability is an urgent task.

Layered double hydroxide (LDH) is a class of clay-like compounds consisting of alternatively stacked positively charged metal hydroxide layers and hydrated interlayer charge-compensating anions.[8] It shows superior thermal and chemical stability as well as rare intrinsic hydroxide ion conductivity, although the ionic conductivities are typically lower than 10^{-3} S/cm.[9,10] Most of the previous studies focused on incorporating LDH nanoparticles into an anion-conductive matrix to enhance the stability and barrier property.[11−13] Being a layered compound, LDH can be exfoliated into two-dimensional (2D) nanosheets. The physical and chemical properties of these 2D nanosheets can be dramatically different from their bulk counterparts and may provide new choices for the design of ionic sieving membranes.[14,15]

In 2017, Sun et al.[16] demonstrated that, when exfoliating bulk LDH into single-layer 2D-LDH nanosheets, its hydroxide ion conductivity can be prominently increased from 10^{-3} to 10^{-1} S/cm, which is comparable with that of commercial proton exchange membranes.[7] This outstanding anionic conductivity, together with superior stability, makes 2D-LDH a promising building block for the construction of future generations of AEMs. Further isotope experiments show that the hydroxide ion transportation mechanism depends on the relative humidity (RH) conditions.[17] At higher RH, the strong isotope effect indicates a Grotthuss-type hydroxide ion

Received: October 21, 2020
Revised: December 20, 2020
Published: January 12, 2021

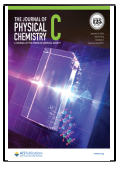

https://dx.doi.org/10.1021/acs.jpcc.0c09517
J. Phys. Chem. C 2021, 125, 1240−1248

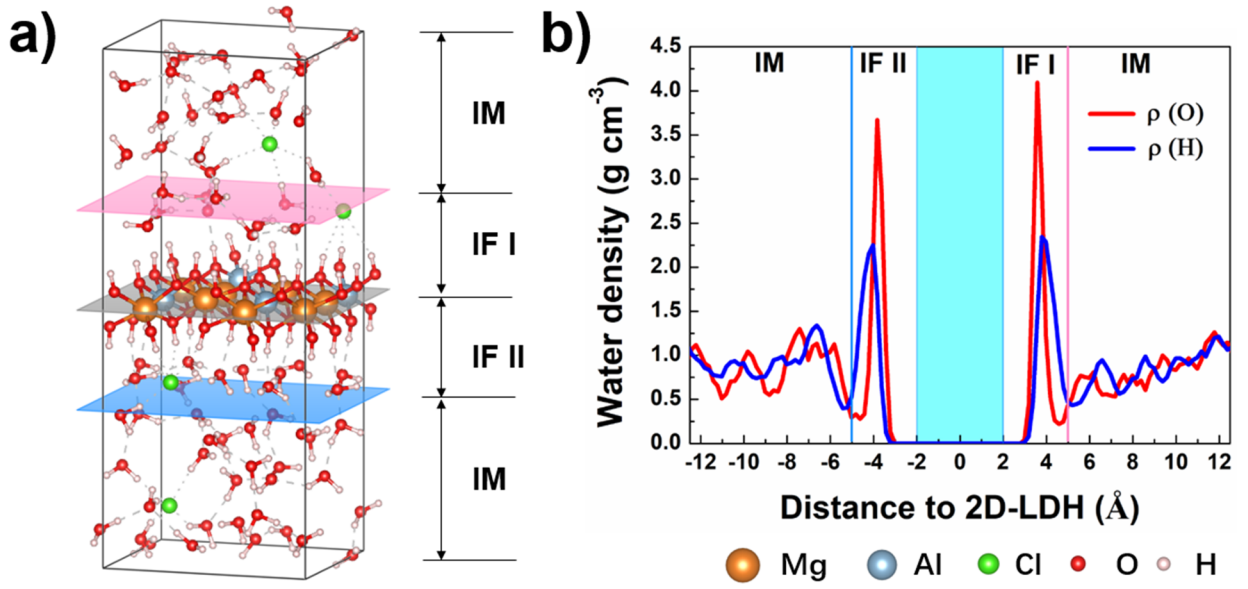

Figure 1. Snapshot and density profile of water as a function of distance to 2D-LDH of the L system. (a) Snapshot of AIMD simulation; here, IM denotes the intermediate region, and IF denotes the interfacial region. (b) Density profile of water, where the light blue area represents 2D-LDH.

conduction,[18] while at lower RH, the hydroxide ion propagation was mainly realized via proton transfer with the surface hydroxyl functional groups of 2D-LDH involved. However, it is experimentally challenging to investigate how the 2D-LDH nanosheets interact with water molecules and how the hydroxyl functional groups and water molecules participate in the hydroxide ion propagation process. On the other hand, previous theoretical explorations mainly focused on a vacuum environment with several water molecules adsorbed using the density functional theory (DFT) approach, which neglects the possible influence of an aqueous environment and temperature.

In this work, we comprehensively investigated the detailed hydroxide ion transportation mechanism along the surface of 2D-LDH nanosheets via performing extensive ab initio molecular dynamics (AIMD) simulations. It is found that the surface hydroxyl functional groups can form a stable hydrogen bonding network with water molecules, and the hydroxide ion exhibits a quasi-two-dimensional conduction behavior along the adjacent layer of water molecules near the positively charged 2D-LDH slab. This result is consistent with previous molecular dynamics simulations on polymeric AEMs, where the hydroxide ion prefers to stay close to the tethered cationic groups.[19] Though the movement of the hydroxide ion along the vertical direction has been restrained, its diffusivity along the 2D-LDH surface is still comparable with that in the bulk water environment. When restacking together, the hydroxide ion diffusivity along the 2D-LDH surface will dramatically decrease, which may be caused by the broken hydrogen bonding network connectivity as well as the increased electrostatic repulsion from interlayer anions induced by the spatial confinement. Surface hydroxyl functional groups of 2D-LDH can bridge the hydroxide ion conduction between two non-adjacent water molecules with a relatively high energy barrier of about 0.15 eV, which can only be activated under low RH conditions. Our computation results explained previous experimental observations and unraveled the hydroxide ion transportation mechanism along the surface of 2D-LDH nanosheets, which will shed light on the design of next-generation AEMs.

2. COMPUTATIONAL METHODOLOGY

Classical MD and AIMD simulations were performed using LAMMPS[20,21] and CP2K[22] software packages, respectively. In classical MD simulations, the ClayFF force field[23,24] was employed. The pressure and temperature damping constants were set to be 1000 and 100 fs for the NPT and NVT in MD simulations. In NPT simulations, the pressure was set to be 1 atm and the temperature was set to be 300 K. In NVT simulations, the temperature was set to be 300 K. In AIMD simulations, ab initio Born−Oppenheimer MD was used for the propagation of classical nuclei. The convergence criterion was set to be 1×10^{-7} a.u. for the optimization of the wave function using the Gaussian and plane wave method, and the wave function was expanded in the Gaussian double zeta with a valence polarization function basis set. An auxiliary basis set of plane waves was used to expand the electron density up to a cutoff of 400 Ry. The core electrons were treated using the Perdew−Burke−Ernzerhof (PBE) gradient correction[25] and Goedecker−Teter−Hutter[26] pseudopotentials. Density functional theory (DFT)-D3 correction[27] was used to account for the van der Waals interaction. All the hydrogen atoms were replaced with deuterium, and a time step of 0.5 fs was adopted. It has been widely reported that DFT calculations with generalized gradient approximation (GGA) functionals yield over-structured liquid under ambient conditions,[28−30] and a temperature around 400 K was necessary for the PBE functional to obtain an oxygen−oxygen pair correlation function comparable with that of the experiment at room temperature.[31] Thus, for the AIMD simulations in the NVT ensemble, the Nośe−Hoover chain thermostat[32] with a time constant of 100 fs was used to keep the temperature at T = 400 K.

The hydrogen bonds were identified using a set of geometric criteria (eq S1). Two molecules are considered to form a hydrogen bond if the distance between the oxygen atoms of these molecules (R_{O-O}) is smaller than 3.3 Å, or the distance

https://dx.doi.org/10.1021/acs.jpcc.0c09517
J. Phys. Chem. C 2021, 125, 1240−1248

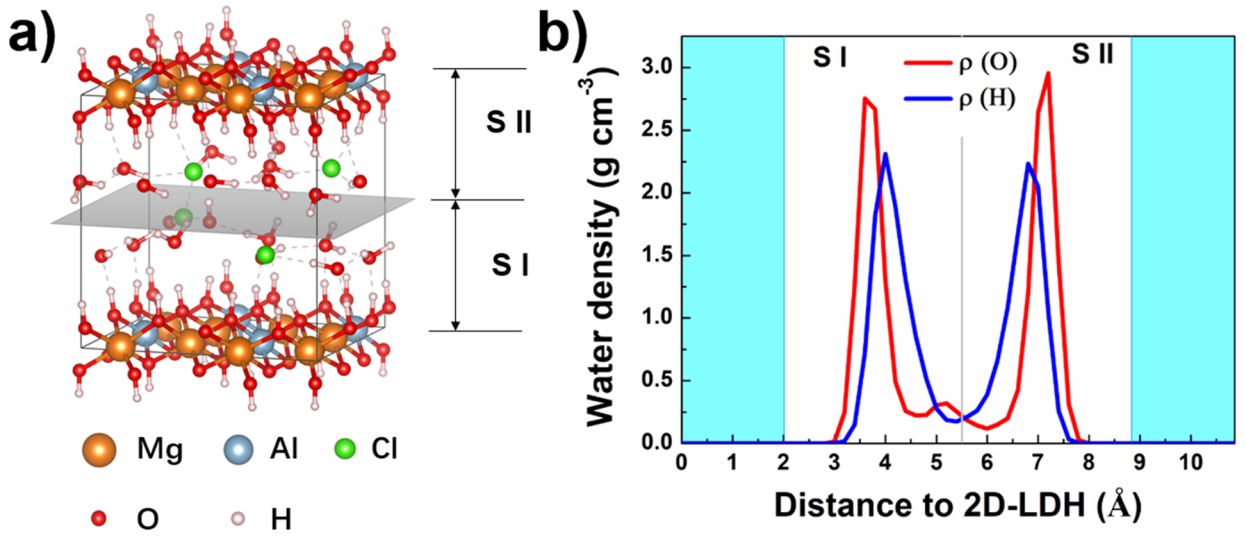

Figure 2. Snapshot and density profile of water as a function of distance to 2D-LDH of the S system. (a) Snapshot of AIMD simulation and (b) density profile of water, where the light blue area represents 2D-LDH.

between the oxygen and chloride atoms of these molecules (R_{O-Cl}) is smaller than 3.8 Å, and at the same time, the angle between the O...O or O...Cl and the O...H vector is less than 30°. The cutoff values of R_{O-O} and R_{O-Cl} are determined based on the radial distribution function obtained from AIMD simulations, as shown in Figure S14.

We defined two variables, $h(t)$ and $H(t)$, to characterize the hydrogen bond dynamics. $h(t)$ is equal to 1 if a particular water pair is hydrogen-bonded and zero otherwise. $H(t) = 1$ indicates that a pair of water molecules remains hydrogen-bonded from $t = 0$ to time t and zero otherwise. The hydrogen bond time correlation function $S_{HB}(t)$ is defined as eq S2

$$S_{HB}(t) = \frac{\langle h(0)H(t)\rangle}{\langle h(0)^2\rangle} \quad \text{(S3)}$$

It gives the probability that an initially hydrogen-bonded pair remains hydrogen-bonded all the time from $t = 0$ to t.

3. RESULTS AND DISCUSSION

3.1. 2D-LDH in the Aqueous Environment. As the hydroxide ion conduction capability of 2D-LDH strongly depends on the humidity conditions, we first investigated the interaction between 2D-LDH and water molecules. One of the most common types of LDH, the $Mg_2Al_1(OH)_6^+$ slab with Cl^- as the counter ion was chosen to construct the simulation systems. A supercell containing a $Mg_8Al_4(OH)_{24}^{4+}$ slab with four Cl^- ions was adopted in our simulation. The interphase between 2D-LDH and water was constructed by putting the 2D-LDH slab and charge-compensating Cl^- ions into a box filled with water molecules with a density of 1 g cm^{-3}. Here, we choose this water density to simulate extreme conditions with high humidity. Then, classical MD simulation in the NPT ensemble ($P = 1$ atm, $T = 300$ K) was performed for 2 ns with x and y directions fixed. Afterward, the system was equilibrated in the NVT ($T = 300$ K) ensemble for another 2 ns. This system was denoted as the "large system (L system)" in the following context, and its detailed configuration after MD equilibration is listed in Table S1. Then, we analyzed the water/2D-LDH interphase by collecting data from both a 1 ns MD simulation and a 20 ps AIMD simulation in the NVT ensemble. Figure 1 shows the snapshot of the L system and the water density distribution obtained from the AIMD simulation. It can be found that the water density distribution shows a peak at about 2 Å away from the surface of 2D-LDH, and the water density after the first peak oscillates around 1 g cm^{-3}. Based on this observation, the aqueous phase was classified into "interfacial (IF)" and "intermediate (IM)" regions (see Figure 1). In Figure S2, we show the trajectory of Cl^- ions as a function of time during the AIMD and MD simulations. It can be found that, for each side of 2D-LDH, there exists two Cl^- ions, and one of the Cl^- ions will stay in the IF region, while the other one prefers to stay in the IM region. Water molecules in the IF region show a clear orientation preference (see Figure S3), which is induced by the hydrogen bonds formed between IF water and the surface hydroxyl functional groups of 2D-LDH. Further analysis of the correlation functions of hydrogen bonds[33] and water dipole,[34] as shown in Figures S4 and S5, reveal that the hydrogen bonds formed between IF water molecules and the surface hydroxyl functional groups of 2D-LDH are more stable than any other type of hydrogen bond in this system.

In practical applications, it is a common practice to stack the exfoliated 2D nanosheets together to form a thin film membrane.[35−37] The interlayer spacing between restacked 2D nanosheets can serve as selective channels for ion transportation. To explore the hydroxide ion transportation behavior in the galleries formed by restacked 2D-LDH, we constructed a "small system (S system)" with an interlayer spacing of 10.86 Å, as shown in Figure 2a (the experimental interlayer spacing of restacked 2D-LDH is about 1.1 nm[16]). The detailed construction protocol is elaborated in the Supporting Information. Figure 2b shows the water density distribution as a function of distance to 2D-LDH obtained from AIMD simulation. It can be found that the water molecules inside the interlayer spacing of 2D-LDH exhibit a clear stratified structure with two density peaks. We classified the water molecules into the SI and SII region based on this stratified structure (see Figure 2a). Figure S7 shows the trajectories of Cl^- as a function of time during the AIMD and MD simulations. For each water layer, two Cl^- ions can be found during the entire simulation time. Similar to the L system, the orientation distribution of water molecules in SI

https://dx.doi.org/10.1021/acs.jpcc.0c09517
J. Phys. Chem. C 2021, 125, 1240−1248

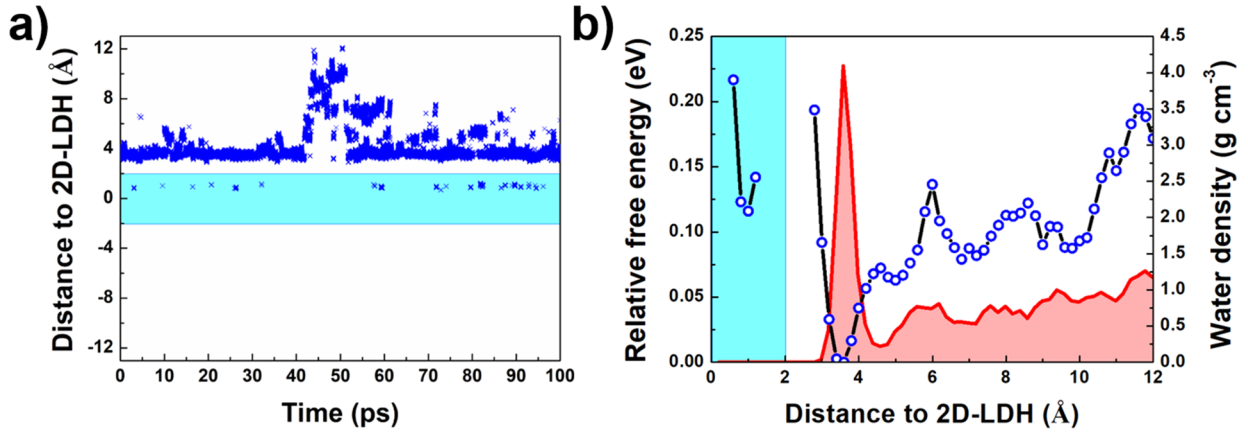

Figure 3. Hydroxide ion diffusion trajectory and energy profile in the L system. (a) Hydroxide ion diffusion trajectory in AIMD simulation. (b) Hydroxide ion energy profile (black line with blue circles) and water density profile (red line with a pink shade) as a function of distance to 2D-LDH. The light blue area represents 2D-LDH.

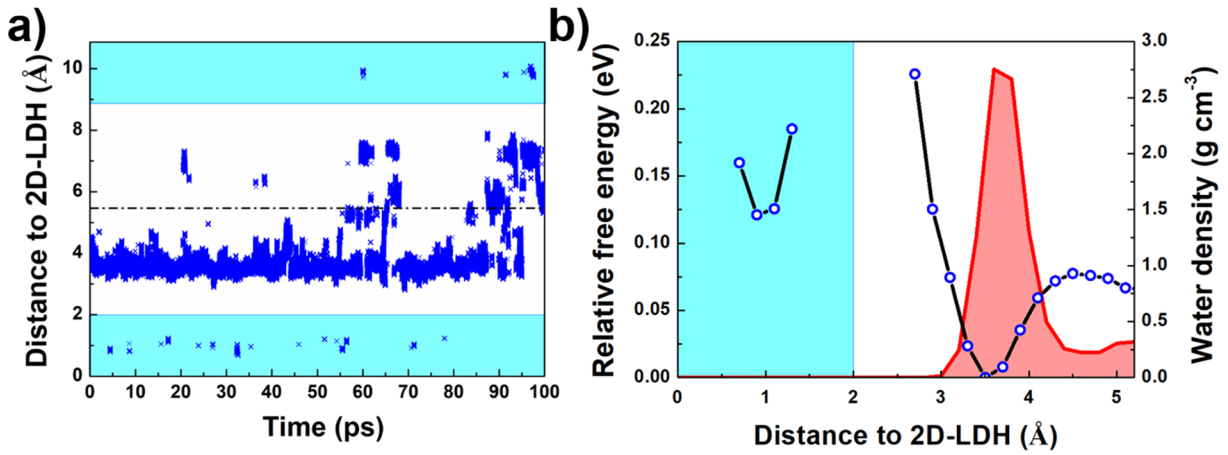

Figure 4. Hydroxide ion diffusion trajectory and energy profile in the S system. (a) Hydroxide ion diffusion trajectory in AIMD simulation. (b) Hydroxide ion energy profile (black line with blue circles) and water density profile (red line with a pink shade) as a function of distance to 2D-LDH. The light blue area represents 2D-LDH.

and SII regions is significantly altered by the surface hydrogen bonds, as shown in Figure S8. The lifetime of hydrogen bonds formed between water molecules and the surface hydroxyl functional groups of 2D-LDH is a bit shorter than that between IF water and 2D-LDH in the L system but still much longer than any other cases, as shown in Figure S4.

3.2. OH^- Distribution near the 2D-LDH Surface. We study the OH^- transportation behavior both along the surface of 2D-LDH and inside the interlayer spacing of 2D-LDH using AIMD simulations. As OH^- in experiments was generated from water hydrolysis, we first replaced one water molecule in the L system with a hydroxide ion and a proton attached to another water molecule. Then, we tracked the trajectories of OH^- and H^+ based on the following rules: (i) if one oxygen atom in the aqueous phase is connected with only one hydrogen atom, then it will be identified as OH^-. (ii) If one of the surface hydroxyl functional groups of 2D-LDH loses its H atom, then the bare O atom in 2D-LDH will be identified as the atom that carries the charge of OH^-. (iii) If one oxygen atom in the aqueous phase is connected with three hydrogen atoms, then it will be identified as the hydronium ion that carries the proton. As shown in Figure S9, OH^- remains close to the 2D-LDH slab, which may be caused by the electrostatic attraction, while H^+ and one of the four Cl^- ions remain far away from the slab before the recombination of OH^- and H^+ occurs at about 13 ps. Thus, to avoid the recombination of OH^- and H^+, which may prevent us from observing the OH^- diffusion property, in the following calculations, H^+ and one of the Cl^- ions were removed from the simulation system. For both the L and S systems, 10 ps AIMD simulations in the NVT ensemble were performed for equilibration. Afterward, the trajectories of OH^- were collected from another two 100 ps AIMD simulations. The OH^- position as a function of time in the L system can be found in Figure 3a, where we can see that OH^- still prefers to stay close to the surface of 2D-LDH. The surface hydroxyl functional groups will occasionally participate in the OH^- propagation procedure by losing its H atom. The time ratio that the surface hydroxyl functional group carries in the charge of OH^- is 0.61% during our simulation, indicating that, in most cases, OH^- prefers to transport among water molecules. Figure 3b shows the free energy profile of OH^- as a function of distance to 2D-LDH, which quantified the free energy required to move a hydroxide ion from one position to another. The free energy profile was calculated based on the following equation[38]

$$F = -k_B T \ln(P_z) \quad (1)$$

https://dx.doi.org/10.1021/acs.jpcc.0c09517
J. Phys. Chem. C 2021, 125, 1240−1248

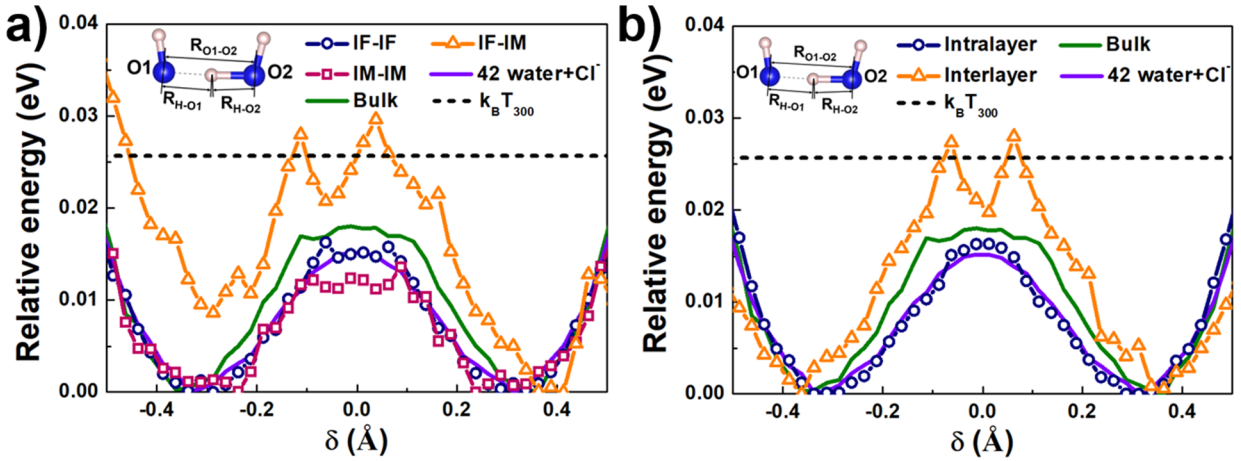

Figure 5. Free energy profiles for proton hole transfer between water molecules in different systems. (a) L system and (b) S system. The data were collected from 100 ps AIMD simulations.

where k_B is the Boltzmann constant, T = 300 K, and P_z is the probability that OH^- appears in a distance of z to 2D-LDH. The lowest energy value was defined as zero. It can be found that the presence of 2D-LDH can confine the OH^- ion in the IF region, and it may serve as a regulator to guide the OH^- transport in the future design of AEMs.

For the S system, the OH^- diffusion trajectory and the corresponding energy profile are shown in Figure 4. It is not surprising to see that OH^- prefers to stay in areas with high water density. Similar to the case of the L system, the surface functional groups of 2D-LDH participate in the OH^- migration process occasionally with a time ratio of 0.65%.

The distance of OH^- relative to its initial position as a function of time in both the L and S system was calculated, as shown in Figure S10. It can be found that, for both the L and S system, a typical burst-and-rest dynamics similar to that in the bulk water environment can be observed,[39] but the migration distance of OH^- in the S system is much shorter than that in the L system. Figure S11 shows the index of oxygen that carries the charge of OH^- as a function of time. Both the Grotthuss and vehicle transportation mechanism contribute to the OH^- migration process in an aqueous environment. When the hydroxyl functional groups of 2D-LDH participate, however, the OH^- migration can only be achieved via Grotthuss hopping between the water molecules and the surface functional groups, which is similar to previous reports.[40−42] The hopping rates of OH^- in L and S systems are 12.26 and 11.36 ps^{-1}, respectively, which are comparable with each other.

The coordinations of OH^- in both L and S systems were analyzed by calculating the radial distribution function of O* (oxygen atom in OH^-) and other oxygen atoms,[43] as shown in Figure S12. In both L and S systems, the coordination number of n_{O^*O} is about 4, which agrees with the previous analysis on the OH^- solvation structure in bulk water.[18] Moreover, one of the coordinated oxygen atoms comes from the surface hydroxyl functional groups of 2D-LDH. These results indicate that the surface hydroxyl functional groups of 2D-LDH can form stable hydrogen bonds with OH^-.

3.3. Proton Hole Transfer between Water Molecules. The elementary OH^- transportation behaviors were investigated by calculating the proton hole transfer energy barriers between different types of water molecules. The proton hole transfer coordinate δ was defined as the distance difference between the proton and its two nearest oxygen atoms O1 and O2 ($\delta = R_{H-O1} - R_{H-O2}$), as illustrated in the insets of Figure 5.[38,44] In addition to the L system, the S system, and a bulk water system containing 64 water molecules (denoted as "bulk water"), a system with 42 water molecules and two Cl^- ions (denoted as the "42 water + Cl^- system") was constructed as well. The Cl^- concentration in the 42water + Cl^- system is the same as that in the IM region of the L system; thus, the possible influence of Cl^- toward the proton hole transfer energy barriers can be examined. Detailed system configurations are listed in Table S1. For proton hole hopping between IF water and IM water in the L system, the oxygen atom of IF water was denoted as O1, and the oxygen atom of IM water was denoted as O2. In other cases, the water molecules are equivalent, and the O1 and O2 index were assigned randomly. Figure 5a shows the energy profiles for proton hole transfer in the L system. It can be found that the proton hole migration energy barriers between IF water molecules, IM water molecules, bulk water molecules, and water molecules in the 42water + Cl^- system are close to each other. While the energy barrier of proton hole hopping between the IF water molecule and IM water molecule is much higher, the energy profile is asymmetric. The asymmetric energy profile suggests that OH^- prefers to stay in the IF region, which agrees with our calculation results shown in Figure 3. It should be noted that Figure 5 shows just the energy profiles of elementary proton hole transfer reactions, while the energy profiles in Figures 3 and 4 are obtained from the statistical results of the OH^- position, which are also influenced by other factors such as water density.

Figure 5b shows the energy profiles of proton hole transfer in the S system. Previous studies suggest that the OH^- conductivity of restacked 2D-LDH is much smaller than that of a single-layer 2D-LDH nanosheet;[15−17] however, we are surprised to see that the energy barrier for proton hole hopping between water molecules in the same layer (intralayer) of the S system is similar to that between bulk water molecules and water molecules in the 42water + Cl^- system. The proton hole hopping energy barrier between water molecules in different layers (interlayer) is similar to the energy barrier between IF and IM water molecules. These results suggest that the spatial confinement did not significantly change the elementary proton hole hopping behavior.

3.4. OH^- Diffusion Coefficient. The OH^- conductivity was determined by the OH^- diffusion property. The OH^-

https://dx.doi.org/10.1021/acs.jpcc.0c09517
J. Phys. Chem. C 2021, 125, 1240−1248

diffusion coefficient in different systems was obtained from five independent AIMD simulations that last 10 ps with different initial geometries, as shown in Figures S13–S16. The calculated diffusion coefficients are listed in Table 1. The

Table 1. Calculated Diffusion Coefficient of OH^- in Different Systems

	L system (D'')	S system (D'')	bulk water (D^{iso})	42water + Cl^- (D^{iso})
D (10^{-5} $cm^2 \cdot s^{-1}$)	18.1	5.0	21.2	20.9

calculated isotropic diffusion coefficient (D^{iso}) of OH^- in bulk water is about 4 times higher than the experimental value (5.4×10^{-5} $cm^2 \cdot s^{-1}$)[45] but agrees with previous calculation results using the PBE functional.[46] The presence of Cl^- in bulk water did not change the OH^- diffusion coefficient. For L and S systems, as the OH^- migration is quasi-two-dimensional, only the lateral mean square displacement (MSD) and diffusion coefficient along the *xy* plane (D'') were calculated. For the L system, though the migration of OH^- is confined in the vertical direction, the lateral diffusion coefficient of OH^- is comparable with that in bulk water. Although OH^- is trapped in the IF region by the presence of the 2D-LDH slab, the lateral migration process is not impeded.

On the other hand, the lateral OH^- diffusion coefficient in the S system is much smaller, which is consistent with the experimentally observed low ionic conductivity of restacked 2D-LDH nanosheets. To explain this phenomenon, we analyzed the hydrogen bonding network formed by water molecules in different systems.[47] The hydrogen bonding status of a water molecule is denoted as A_iD_j, meaning that this water molecule accepts i hydrogen bonds and donates j hydrogen bonds (i, j = 2, 1, or 0). Figure 6 shows the hydrogen bond statistics only considering hydrogen bonds formed between water molecules. The hydrogen bond statistics of the IM region in the L system are similar to those of the 42water + Cl^- system, as shown in Figure S18, suggesting that the influence of 2D-LDH toward IM water is weak. However, different from IM water, the A_1D_2 structure is the most popular hydrogen bonding status for IF water molecules. This is caused by the fact that most of the IF water molecules accept a hydrogen bond from 2D-LDH, which can be validated by the hydrogen bond statistics considering all kinds of hydrogen bonds, as shown in Figure S19 and Table S4. For the S system, the hydrogen bond statistics of water molecules are dramatically different from both the IF and IM regions of the L system. Water molecules with the hydrogen bonding status of A_0D_0, A_0D_1, and A_1D_0 account for half of the total number of water molecules. As OH^- mainly propagates among water molecules via the Grotthuss mechanism,[18] only a connected hydrogen bond network can realize a long-distance OH^- migration. The water molecules with the hydrogen bonding status of A_0D_0, A_0D_1, and A_1D_0 can be regarded as an isolated point or the end of the hydrogen bonding network and cannot pass OH^- further, as shown in Figure S20. As listed in Table S4, only half the amount of the hydrogen bonds in the S system is formed between water molecules. Compared with the hydrogen bonding network in the IF region, the spatial confinement of restacked 2D-LDH increases the ratio of hydrogen bonds formed between water molecules and the Cl^- ion. Consequently, though with a low proton hole hopping energy barrier, OH^- can only rattle among several water molecules in a localized area in the S system, which significantly hampered its diffusion capability. On the other hand, the spatial confinement will also enhance the electrostatic repulsion between OH^- and Cl^-, which will further decrease the OH^- diffusivity. Figures S21 and S22 show the distance of OH^- and Cl^- ions relative to their initial position as a function of time in both the L and S system. It can be found that the migration property of Cl^- ions does not seem to be significantly affected by the spatial confinement, while the OH^- migration capability of OH^- in the S system is significantly reduced.

3.5. 2D-LDH-Mediated OH^- Migration. In Figures 3 and 4, we found that the surface hydroxyl functional groups of 2D-LDH can occasionally participate in the OH^- migration process. Detailed inspection of the OH^- migration process reveals that only the proton hole hopping between 2D-LDH surface hydroxyl functional groups and IF water molecules can be observed. Namely, the proton hole cannot directly transport between the surface hydroxyl functional groups. Here, we denote surface hydroxyl oxygen as O1 and water oxygen as O2. The proton hole transfer coordinate δ ($\delta = R_{H-O1} - R_{H-O2}$) was calculated and analyzed. The proton hole hopping energy profiles between water molecules and surface hydroxyl functional groups of 2D-LDH in both L and S systems are

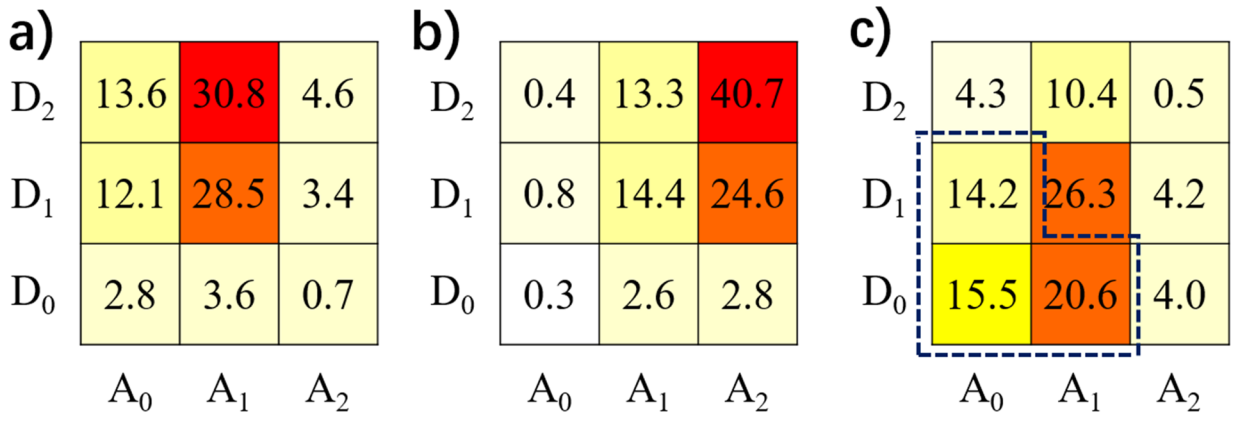

Figure 6. Hydrogen bond statistics of water molecules in different systems. (a) IF region in the L system, (b) IM region in the L system, and (c) S system. The digital numbers in the square represent percentage (%) of corresponding water molecules that accept and/or donate i = 2, 1, or 0 H-bonds denoted by A_i and D_i, respectively. Only hydrogen bonds formed between water molecules were considered.

https://dx.doi.org/10.1021/acs.jpcc.0c09517
J. Phys. Chem. C 2021, 125, 1240−1248

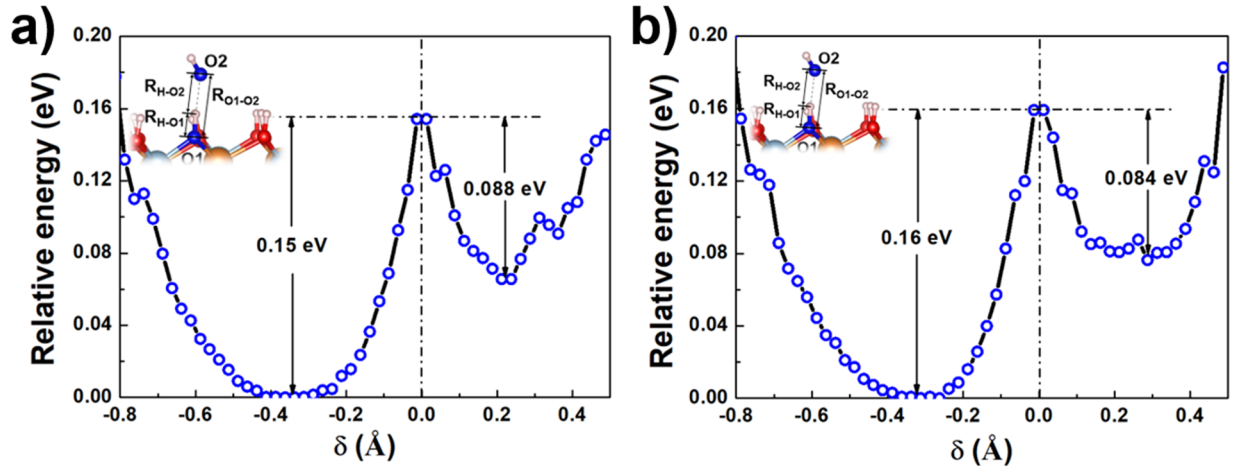

Figure 7. Free energy profiles for proton hole transfer between the surface hydroxyl functional groups of 2D-LDH and water molecule in (a) the L system and (b) the S system.

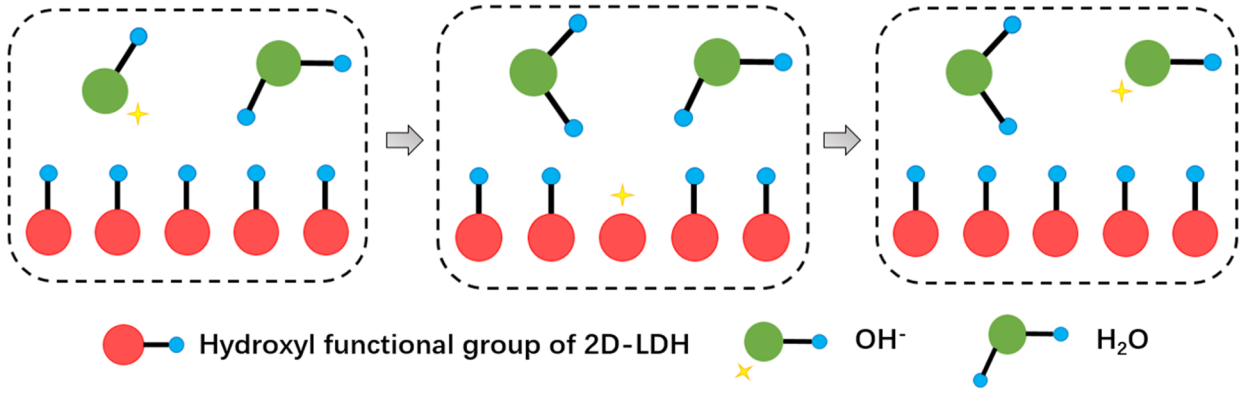

Figure 8. Proposed surface hydroxyl functional group mediated the hydroxide ion propagation scenario in low RH conduction.

shown in Figure 7. It can be found that the spatial confinement of restacking shows little influence toward the proton hole hopping energy barriers. The asymmetric energy profiles suggest that OH^- in the aqueous phase is a more stable state. Extracting one hydrogen atom from the surface hydroxyl functional groups needs to overcome an energy barrier of about 0.15 eV.

In aqueous or high RH conditions, as suggested by our calculations, OH^- mainly propagates via the Grotthuss mechanism among water molecules and the participation of surface hydroxyl functional groups of 2D-LDH is not indispensable. In low RH conditions, however, the involvement of 2D-LDH surface functional groups may become important. As illustrated in Figure 8, the surface hydroxyl functional group can mediate the proton hole transportation between non-adjacent water molecules and makes the long-distance OH^- migration possible, which is similar to our previously proposed water-mediated proton transportation along the surface of GO nanosheets.[48] This proposed mechanism perfectly explained the experimentally observed weak isotope effect and much lower OH^- conductance of 2D-LDH in a low RH environment.

4. CONCLUSIONS

In summary, our AIMD simulation results show that water molecules near the surface of 2D-LDH play a vital role in OH^- transportation in aqueous or a high RH environment. OH^- will be trapped in the first adsorbed layer of water molecules near the surface of 2D-LDH, and it will then migrate along the 2D-LDH surface with a diffusion coefficient comparable with that of bulk water. Restacking 2D-LDH will not significantly influence the elementary OH^- hopping energy barriers but will result in a much lower diffusion coefficient due to the detriment of the hydrogen bond network connectivity. The surface hydroxyl functional groups can participate in the OH^- propagation process with a relatively high OH^- hopping energy barrier of 0.15 eV, which can only be activated in low RH conditions.

Our work elucidated the OH^- propagation mechanism along the surface of 2D-LDH nanosheets. The high lateral diffusion coefficient of OH^- along the surface of 2D-LDH verified the feasibility of using 2D-LDH as a building block for future AEMs. When restacking the exfoliated 2D-LDH nanosheets, the interlayer distance needs to be tuned explicitly by functionalization or intercalation to enlarge the interlayer spacing and maintain the superionic conductivity.[9,49,50] Low RH operation conditions should be avoided in general. However, in some circumstances that do not require a high OH^- conductance, 2D-LDH can still function as a stable OH^- conductor.

https://dx.doi.org/10.1021/acs.jpcc.0c09517
J. Phys. Chem. C 2021, 125, 1240−1248

■ ASSOCIATED CONTENT

Supporting Information

The Supporting Information is available free of charge at https://pubs.acs.org/doi/10.1021/acs.jpcc.0c09517.

Calculation details of water density distribution, H-bond correlation function, dipole correlation function, and diffusion coefficient; protocol to construct the S system; water density distribution, Cl^- trajectories, distribution of angle formed between the OH bond and the *xy* plane, time dependence of H-bond correlation functions, and time dependence of dipole correlation functions in L and S systems; proton and hydroxide ion diffusion trajectory in the L system before recombination; radial distribution function of oxygen atoms and hydroxide oxygen in L and S systems; mean square displacement of OH^- in different systems; oxygen−oxygen and oxygen−chloride radial distribution function in the 42water + Cl^- system; hydrogen bond statistics of water molecules in different systems; snapshots of the hydrogen bonding network; detailed system configurations; hydrogen bond lifetime of L and S systems; and hydrogen bond analysis for different systems (PDF)

■ AUTHOR INFORMATION

Corresponding Author

Le Shi − *State Key Laboratory of Electrical Insulation and Power Equipment, Center of Nanomaterials for Renewable Energy, School of Electrical Engineering, Xi'an Jiaotong University, Xi'an 710049, China;* orcid.org/0000-0003-1468-4549; Email: le.shi@mail.xjtu.edu.cn

Authors

Zhixuan Ying − *State Key Laboratory of Electrical Insulation and Power Equipment, Center of Nanomaterials for Renewable Energy, School of Electrical Engineering, Xi'an Jiaotong University, Xi'an 710049, China*

Ao Xu − *School of Aeronautics, Northwestern Polytechnical University, Xi'an 710072, China*

Yonghong Cheng − *State Key Laboratory of Electrical Insulation and Power Equipment, Center of Nanomaterials for Renewable Energy, School of Electrical Engineering, Xi'an Jiaotong University, Xi'an 710049, China*

Complete contact information is available at: https://pubs.acs.org/10.1021/acs.jpcc.0c09517

Author Contributions

L.S. conceived the research and designed the numerical simulations; L.S., Z.Y., and A.X. analyzed the data; L.S. wrote the paper; and L.S., Z.Y., A.X., and Y.C. discussed the manuscript.

Notes

The authors declare no competing financial interest.

■ ACKNOWLEDGMENTS

The authors acknowledge the Beijing Super Cloud Computing Center (BSCC) and Beijing Beilong Super Cloud Computing Co., Ltd. for providing HPC resources that have contributed to the research results reported within this paper. The authors also acknowledge the HPC Platform, Xi'an Jiaotong University. The work described in this paper was supported by the National Natural Science Foundation of China (51907159) and the Young Talent Recruiting Plans of Xi'an Jiaotong University (DQ6J002).

■ REFERENCES

(1) Merle, G.; Wessling, M.; Nijmeijer, K. Anion Exchange Membranes for Alkaline Fuel Cells: A Review. *J. Membr. Sci.* **2011**, *377*, 1−35.

(2) Hagesteijn, K. F. L.; Jiang, S.; Ladewig, B. P. A Review of the Synthesis and Characterization of Anion Exchange Membranes. *J. Mater. Sci.* **2018**, *53*, 11131−11150.

(3) Ran, J.; Wu, L.; He, Y.; Yang, Z.; Wang, Y.; Jiang, C.; Ge, L.; Bakangura, E.; Xu, T. Ion Exchange Membranes: New Developments and Applications. *J. Membr. Sci.* **2017**, *522*, 267−291.

(4) Gottesfeld, S.; Dekel, D. R.; Page, M.; Bae, C.; Yan, Y.; Zelenay, P.; Kim, Y. S. Anion Exchange Membrane Fuel Cells: Current Status and Remaining Challenges. *J. Power Sources* **2018**, *375*, 170−184.

(5) Yang, Z.; Ran, J.; Wu, B.; Wu, L.; Xu, T. Stability Challenge in Anion Exchange Membrane for Fuel Cells. *Curr. Opin. Chem. Eng.* **2016**, *12*, 22−30.

(6) Marino, M. G.; Kreuer, K. D. Alkaline Stability of Quaternary Ammonium Cations for Alkaline Fuel Cell Membranes and Ionic Liquids. *ChemSusChem* **2015**, *8*, 513−523.

(7) Peighambardoust, S. J.; Rowshanzamir, S.; Amjadi, M. Review of the Proton Exchange Membranes for Fuel Cell Applications. *Int. J. Hydrogen Energy* **2010**, *35*, 9349−9384.

(8) Laipan, M.; Yu, J.; Zhu, R.; Zhu, J.; Smith, A. T.; He, H.; O'Hare, D.; Sun, L. Functionalized Layered Double Hydroxides for Innovative Applications. *Mater. Horiz.* **2020**, *7*, 715−745.

(9) Kubo, D.; Tadanaga, K.; Hayashi, A.; Tatsumisago, M. Hydroxide Ion Conduction in Ni-Al Layered Double Hydroxide. *J. Electroanal. Chem.* **2012**, *671*, 102−105.

(10) Nieto-Malagön, G.; Cuautli, C.; Ireta, J. Interlaminar Anionic Transport in Layered Double Hydroxides: Estimation of Diffusion Coefficients. *J. Phys. Chem. C* **2018**, *122*, 171−176.

(11) Zeng, L.; Zhao, T. S.; Li, Y. S. Synthesis and Characterization of Crosslinked Poly (vinyl alcohol)/Layered Double Hydroxide Composite Polymer Membranes for Alkaline Direct Ethanol Fuel Cells. *Int. J. Hydrogen Energy* **2012**, *37*, 18425−18432.

(12) Kubo, D.; Tadanaga, K.; Hayashi, A.; Tatsumisago, M. Improvement of Electrochemical Performance in Alkaline Fuel Cell by Hydroxide Ion Conducting Ni-Al Layered Double Hydroxide. *J. Power Sources* **2013**, *222*, 493−497.

(13) Xu, X.; Wang, L.; Wang, J.; Yin, Q.; Dong, S.; Han, J.; Wei, M. Hydroxide-Ion-Conductive Gas Barrier Films Based on Layered Double Hydroxide/Polysulfone Multilayers. *Chem. Commun.* **2018**, *54*, 7778−7781.

(14) Liu, G.; Jin, W.; Xu, N. Two-Dimensional-Material Membranes: A New Family of High-Performance Separation Membranes. *Angew. Chem., Int. Ed.* **2016**, *55*, 13384−13397.

(15) Sun, P.; Ma, R.; Sasaki, T. Recent Progress on Exploring Exceptionally High and Anisotropic H^+/OH^- Ion Conduction in Two-Dimensional Materials. *Chem. Sci.* **2018**, *9*, 33−43.

(16) Sun, P.; Ma, R.; Bai, X.; Wang, K.; Zhu, H.; Sasaki, T. Single-Layer Nanosheets with Exceptionally High and Anisotropic Hydroxyl Ion Conductivity. *Sci. Adv.* **2017**, *3*, No. e1602629.

(17) Sun, P.; Chen, F.; Zhou, W.; Liu, X.; Ma, R.; Sasaki, T. Superionic Conduction Along Ordered Hydroxyl Networks in Molecular-Thin Nanosheets. *Mater. Horiz.* **2019**, *6*, 2087−2093.

(18) Marx, D.; Chandra, A.; Tuckerman, M. E. Aqueous Basic Solutions: Hydroxide Solvation, Structural Diffusion, and Comparison to the Hydrated Proton. *Chem. Rev.* **2010**, *110*, 2174−2216.

(19) Chen, C.; Tse, Y. L. S.; Lindberg, G. E.; Knight, C.; Voth, G. A. Hydroxide Solvation and Transport in Anion Exchange Membranes. *J. Am. Chem. Soc.* **2016**, *138*, 991−1000.

(20) Plimpton, S. Fast Parallel Algorithms for Short-Range Molecular Dynamics. *J. Comput. Phys.* **1995**, *117*, 1−9.

(21) Aktulga, H. M.; Fogarty, J. C.; Pandit, S. A.; Grama, A. Y. Parallel Reactive Molecular Dynamics: Numerical Methods and Algorithmic Techniques. *Parallel Comput.* **2012**, *38*, 245−259.

(22) VandeVondele, J.; Krack, M.; Mohamed, F.; Parrinello, M.; Chassaing, T.; Hutter, J. Quickstep: Fast and Accurate Density Functional Calculations Using a Mixed Gaussian and Plane Waves Approach. *Comput. Phys. Commun.* **2005**, *167*, 103−128.
(23) Cygan, R. T.; Liang, J. J.; Kalinichev, A. G. Molecular Models of Hydroxide, Oxyhydroxide, and Clay Phases and the Development of a General Force Field. *J. Phys. Chem. B* **2004**, *108*, 1255−1266.
(24) Pouvreau, M.; Greathouse, J. A.; Cygan, R. T.; Kalinichev, A. G. Structure of Hydrated Gibbsite and Brucite Edge Surfaces: DFT Results and Further Development of the ClayFF Classical Force Field with Metal-O-H Angle Bending Terms. *J. Phys. Chem. C* **2017**, *121*, 14757−14771.
(25) Perdew, J. P.; Ernzerhof, M.; Burke, K. Rationale for Mixing Exact Exchange with Density Functional Approximations. *J. Chem. Phys.* **1996**, *105*, 9982−9985.
(26) Goedecker, S.; Teter, M.; Hutter, J. Separable Dual-Space Gaussian Pseudopotentials. *Phys. Rev. B* **1996**, *54*, 1703.
(27) Grimme, S.; Antony, J.; Ehrlich, S.; Krieg, H. A Consistent and Accurate Ab Initio Parametrization of Density Functional Dispersion Correction (DFT-D) for the 94 Elements H-Pu. *J. Chem. Phys.* **2010**, *132*, 154104.
(28) Pham, T. A.; Ogitsu, T.; Lau, E. Y.; Schwegler, E. Structure and Dynamics of Aqueous Solutions from PBE-Based First-Principles Molecular Dynamics Simulations. *J. Chem. Phys.* **2016**, *145*, 154501.
(29) VandeVondele, J.; Mohamed, F.; Krack, M.; Hutter, J.; Sprik, M.; Parrinello, M. The Influence of Temperature and Density Functional Models in Ab Initio Molecular Dynamics Simulation of Liquid Water. *J. Chem. Phys.* **2005**, *122*, No. 014515.
(30) Brorsen, K. R.; Willow, S. Y.; Xantheas, S. S.; Gordon, M. S. The Melting Temperature of Liquid Water with the Effective Fragment Potential. *J. Phys. Chem. Lett.* **2015**, *6*, 3555−3559.
(31) Shi, L.; Xu, A.; Pan, D.; Zhao, T. Aqueous Proton-Selective Conduction Across Two-Dimensional Graphyne. *Nat. Commun.* **2019**, *10*, 1−8.
(32) Evans, D. J.; Holian, B. L. The Nose−Hoover Thermostat. *J. Chem. Phys.* **1985**, *83*, 4069−4074.
(33) Bankura, A.; Karmakar, A.; Carnevale, V.; Chandra, A.; Klein, M. L. Structure, Dynamics, and Spectral Diffusion of Water from First-Principles Molecular Dynamics. *J. Phys. Chem. C* **2014**, *118*, 290401−229411.
(34) Cicero, G.; Grossman, J. C.; Schwegler, E.; Gygi, F.; Galli, G. Water Confined in Nanotubes and Between Graphene Sheets: A First Principle Study. *J. Am. Chem. Soc.* **2008**, *130*, 1871−1878.
(35) Mi, B. Graphene Oxide Membranes for Ionic and Molecular Sieving. *Science* **2014**, *343*, 740−742.
(36) Ries, L.; Petit, E.; Michel, T.; Diogo, C. C.; Gervais, C.; Salameh, C.; Bechelany, M.; Balme, S.; Miele, P.; Onofrio, N.; et al. Enhanced Sieving from Exfoliated MoS2 Membranes via Covalent Functionalization. *Nat. Mater.* **2019**, *18*, 1112−1117.
(37) Raidongia, K.; Huang, J. Nanofluidic Ion Transport Through Reconstructed Layered Materials. *J. Am. Chem. Soc.* **2012**, *134*, 16528−16531.
(38) Munoz-Santiburcio, D.; Marx, D. On the Complex Structural Diffusion of Proton Holes in Nanoconfined Alkaline Solutions Within Slit Pores. *Nat. Commun.* **2016**, *7*, 1−9.
(39) Tse, Y. L. S.; Knight, C.; Voth, G. A. An Analysis of Hydrated Proton Diffusion in Ab Initio Molecular Dynamics. *J. Chem. Phys.* **2015**, *142*, No. 014104.
(40) Ludueña, G. A.; Kühne, T. D.; Sebastiani, D. Mixed Grotthuss and Vehicle Transport Mechanism in Proton Conducting Polymers from Ab Initio Molecular Dynamics Simulations. *Chem. Mater.* **2011**, *23*, 1424−1429.
(41) Chen, M.; Shen, W.; Lu, X.; Zhu, R.; He, H.; Zhu, J. Jumping Diffusion of Water Intercalated in Layered Double Hydroxides. *J. Phys. Chem. C* **2016**, *120*, 12924−12931.
(42) Chen, M.; Zhu, R.; Zhu, J.; He, H. Temperature-Dependent Structure and Dynamics of Water Intercalated in Layered Double Hydroxides with Different Hydration States. *J. Phys. Chem. C* **2017**, *121*, 23752−23762.
(43) Grosjean, B.; Bocquet, M. L.; Vuilleumier, R. Versatile Electrification of Two-Dimensional Nanomaterials in Water. *Nat. Commun.* **2019**, *10*, 1−8.
(44) Bankura, A.; Chandra, A. Proton Transfer Through Hydrogen Bonds in Two-Dimensional Water Layers: A Theoretical Study Based on Ab Initio and Quantum-Classical Simulations. *J. Chem. Phys.* **2015**, *142*, No. 044701.
(45) Halle, B.; Karlström, G. Prototropic Charge Migration in Water. Part 2.-Interpretation of Nuclear Magnetic Resonance and Conductivity Data in Terms of Model Mechanisms. *J. Chem. Soc., Faraday Trans.* **1983**, *79*, 1047−1073.
(46) Chen, M.; Zheng, L.; Santra, B.; Ko, H. Y.; DiStasio, R. A., Jr.; Klein, M. L.; Car, R.; Wu, X. Hydroxide Diffuses Slower Than Hydronium in Water Because Its Solvated Structure Inhibits Correlated Proton Transfer. *Nat. Chem.* **2018**, *10*, 413−419.
(47) Ruiz-Barragan, S.; Muñoz-Santiburcio, D.; Marx, D. Nano-confined Water Within Graphene Slit Pores Adopts Distinct Confinement-Dependent Regimes. *J. Phys. Chem. Lett.* **2018**, *10*, 329−334.
(48) Shi, L.; Ying, Z.; Xu, A.; Cheng, Y. Unravelling the Water Mediated Proton Conduction Mechanism Along the Surface of Graphene Oxide. *Chem. Mater.* **2020**, *32*, 6062−6069.
(49) Furukawa, Y.; Tadanaga, K.; Hayashi, A.; Tatsumisago, M. Evaluation of Ionic Conductivity for Mg-Al Layered Double Hydroxide Intercalated with Inorganic Anions. *Solid State Ionics* **2011**, *192*, 185−187.
(50) He, X.; Cao, L.; He, G.; Zhao, A.; Mao, X.; Huang, T.; Li, Y.; Wu, H.; Sun, J.; Jiang, Z. A Highly Conductive and Robust Anion Conductor Obtained via Synergistic Manipulation in Intra-and Inter-Laminate of Layered Double Hydroxide Nanosheets. *J. Mater. Chem. A* **2018**, *6*, 10277−10285.

https://dx.doi.org/10.1021/acs.jpcc.0c09517
J. Phys. Chem. C 2021, 125, 1240−1248